Exp Brain Res (2008) 187:551–561
DOI 10.1007/s00221-008-1318-8

RESEARCH ARTICLE

Ultra-high field parallel imaging of the superior parietal lobule during mental maze solving

Trenton A. Jerde · Scott M. Lewis · Ute Goerke · Pavlos Gourtzelidis · Charidimos Tzagarakis · Joshua Lynch · Steen Moeller · Pierre-François Van de Moortele · Gregor Adriany · Jeran Trangle · Kâmil Uğurbil · Apostolos P. Georgopoulos

Received: 5 December 2007 / Accepted: 11 February 2008 / Published online: 28 February 2008

Abstract We used ultra-high field (7 T) fMRI and parallel imaging to scan the superior parietal lobule (SPL) of human subjects as they mentally traversed a maze path in one of four directions (up, down, left, right). A counterbalanced design for maze presentation and a quasi-isotropic voxel (1.46 × 1.46 × 2 mm thick) collection were implemented. Fifty-one percent of single voxels in the SPL were tuned to the direction of the maze path. Tuned voxels were distributed throughout the SPL, bilaterally. A nearest neighbor analysis revealed a "honeycomb" arrangement such that voxels tuned to a particular direction tended to occur in clusters. Three-dimensional (3D) directional clusters were identified in SPL as oriented centroids traversing the cortical depth. There were 13 same-direction clusters per hemisphere containing 22 voxels per cluster, on the average; the mean nearest-neighbor, same-direction intercluster distance was 9.4 mm. These results provide a much finer detail of the directional tuning in SPL, as compared to those obtained previously at 4 T (Gourtzelidis et al. Exp Brain Res 165:273–282, 2005). The more accurate estimates of quantitative clustering parameters in 3D brain space in this study were made possible by the higher signal-to-noise and contrast-to-noise ratios afforded by the higher magnetic field of 7 T as well as the quasi-isotropic design of voxel data collection.

Keywords Ultra-high field fMRI · Superior parietal lobule · Directional tuning · Spatial cognition · Parallel imaging

T. A. Jerde · U. Goerke · S. Moeller · P.-F. Van de Moortele · G. Adriany · K. Uğurbil
Center for Magnetic Resonance Research, Department of Radiology, University of Minnesota Medical School, Minneapolis, MN 55455, USA

S. M. Lewis · P. Gourtzelidis · C. Tzagarakis · J. Lynch · J. Trangle · A. P. Georgopoulos (✉)
Brain Sciences Center, Veterans Affairs Medical Center, Minneapolis, MN 55417, USA
e-mail: omega@umn.edu

S. M. Lewis · A. P. Georgopoulos
Department of Neuroscience, University of Minnesota Medical School, Minneapolis, MN 55455, USA

S. M. Lewis · A. P. Georgopoulos
Department of Neurology, University of Minnesota Medical School, Minneapolis, MN 55455, USA

A. P. Georgopoulos
Department of Psychiatry, University of Minnesota Medical School, Minneapolis, MN 55455, USA

A. P. Georgopoulos
Center for Cognitive Sciences, University of Minnesota, Minneapolis, MN 55455, USA

Introduction

Technical developments in functional magnetic resonance imaging (fMRI) that improve the signal-to-noise ratio (SNR), contrast-to-noise ratio (CNR), and spatial specificity of the signal are essential for the continued efficacy of fMRI as a research tool in cognitive neuroscience. The vast majority of fMRI studies rely on T_2* blood oxygen level-dependent (BOLD) contrast. BOLD contrast originates from the intravoxel inhomogeneity induced by paramagnetic deoxyhemaglobin sequestered in red blood cells, which are themselves compartmentalized within blood vessels. Increasing the field strength of the main magnetic field (B_0) increases the bulk susceptibility difference between blood containing deoxyhemoglobin and the surrounding diamagnetic tissue, and thereby yields

greater MR signal change in a task condition compared to baseline (Gati et al. 1999). The increase in sensitivity with high magnetic fields has been demonstrated in numerous studies (Turner et al. 1993; Gati et al. 1997; Krüger et al. 2001; Yacoub et al. 2001; Krasnow et al. 2003; Fera et al. 2004; Zou et al. 2005). The most important benefit of using ultra-high fields, however, is the increase in spatial specificity—that is, the correspondence between the MR signal and the underlying neuronal response (Uğurbil 2002; Uğurbil et al. 2003, 2006). At 1.5 T and even at 3 T, increased neuronal activity can induce BOLD signal changes from large blood vessels that do not co-localize with the site of neuronal activity (Menon et al. 1993; Segebarth et al. 1994). Moreover, the BOLD signal from the microvasculature (i.e., the capillaries and small post-capillary venules), which is of most interest to researchers, is largely undetectable at 1.5 T and deluged by large vessel contributions at 3 T. At ultra-high fields such as 7 T, however, the nonspecific BOLD signal from large vessels is reduced (Yacoub et al. 2001, 2005) because the venous blood T_2 decreases with increasing magnetic field (Duong et al. 2003). Furthermore, the BOLD signal from the microvasculature increases approximately quadratically with field strength and is substantially enhanced at 7 T (Yacoub et al. 2005).

Despite the benefits of ultra-high field fMRI, it presents challenges, such as increased inhomogeneity of B_0, reduced T_2 and T_2* relaxation times, increased electromagnetic energy absorbed by the tissue (SAR), and increased scanner noise. These challenges can be offset by combining ultra-high field fMRI with parallel imaging (Wiesinger et al. 2004, 2006; Moeller et al. 2006). In parallel imaging, multiple receiver coils simultaneously acquire spatial information from different regions of the object being imaged, rather than relying on the switching of magnetic field gradients for spatial encoding (Sodickson et al. 1997; Pruessman et al. 1999). The advantages of parallel imaging include reduced acquisition time, potentially higher spatial and temporal resolution, reduced artifacts due to B_0 inhomogeneity and motion, reduced SAR, and reduced scanner noise. A limitation of parallel imaging is a decrease in SNR due to less sampling of the *k*-space data and unaliasing, but this loss in SNR is often less than the loss of CNR (Moeller et al. 2006 and references therein) depending on the contributions of intrinsic and physiological noise. But since an increase in SNR is a major benefit of ultra-high field fMRI, the advantages and limitations of ultra-high field fMRI and parallel imaging complement each other.

In terms of applications, ultra-high field fMRI and parallel imaging enable cognitive neuroscientists to perform experiments on more specific attributes of sensory, cognitive, and motor processes, and to be more confident that the observed loci of activation co-localize with the area of increased neuronal activity. In the present study, we used a 7 T magnet and parallel imaging with a one-dimensional reduction factor of 4 (Moeller et al. 2006) and a 15-channel coil (Adriany et al. 2004) to scan the human SPL during a maze task in which the direction of covert attention was investigated. Covert attention refers to the allocation of attention in the absence of eye movements. The SPL is a crucial area within the human posterior parietal cortex (PPC) for visuospatial functions such as mental rotation (Richter et al. 2000; Tagaris et al. 2000) and visuospatial attention (Corbetta et al. 1993; Vandenberghe et al. 2001; Fan et al. 2005; Molenberghs et al. 2007). Maze tasks have an extensive history in psychology and neuroscience as a probe of spatial processing (Tolman 1932; Porteus 1969; Olton 1979; Brown et al. 1999). Recent studies in monkeys (Crowe et al. 2004, 2005; Nitz 2006) and humans (Gourtzelidis et al. 2005) have identified the PPC as a critical area for the spatial processing that is requisite in solving mazes.

In a previous study of maze solving using 4 T fMRI (Gourtzelidis et al. 2005), we observed tuning of single voxels in the SPL with respect to the direction in which a maze was mentally traversed. Furthermore, tuned voxels with similar preferred directions tended to cluster, and patches of tuned voxels with different preferred directions were distributed throughout the SPL. This study demonstrated that direction is a critical attribute in the neural control of attention, and furthermore, that it can be detected by fMRI at the single-voxel level. These results are consistent with an optical imaging study of monkeys (Raffi and Siegel 2005), in which the locus of spatial attention was correlated with a patchy topological arrangement in the inferior parietal lobe (IPL), an area believed to be homologous to the human SPL. In the present study, we utilized an experimental design in which the direction of covert visual attention was manipulated throughout the experiment, without a typical baseline condition that differed appreciably from the task condition. This design ensured that the activation of single voxels was due to the direction of attention and not to extraneous factors, such as the difference in the level of attention between task and control conditions (Scannell and Young 1999).

Materials and methods

Subjects

Data were obtained from three healthy, right-handed subjects (two men and one woman, ages 23–43) who participated in the study as paid volunteers. The institutional review board at the University of Minnesota approved the protocol. Informed consent was obtained

from all subjects prior to the study according to the Declaration of Helsinki.

Stimuli and tasks

Mazes were generated by a computer and presented to subjects via a rear-projection screen and a mirror attached to the coil. Mazes were composed of white lines on a black background and subtended $\sim 5° \times 5°$ of visual angle. Subjects mentally traversed one of four radially directed paths (up, down, left, right) of a maze while fixating a central point (Fig. 1). Mazes were filled with random linear distracters except for the non-branching central path that extended in one of the four directions. Half of the radial paths were open-ended and exited the maze ("exit" mazes), and half were closed by a line near the end of the maze ("no-exit" mazes); the exit status of each maze was selected randomly by the computer. Subjects pressed one of two buttons with their right hand to indicate whether the maze path had an exit or not. To prevent subjects from being able to judge the exit status of a maze by the mere presence of a gap in the perimeter of exit mazes, two additional gaps (for a total of three) were added at random locations in the perimeter. No-exit mazes did not have gaps, so three gaps were randomly added to the maze perimeter to keep the number of gaps constant for exit and no-exit mazes.

A block design was used such that 35 mazes (trials) of a given direction were presented in 42-s blocks. A trial lasted 1.2 s, with the maze displayed for the first 300 ms. This brief presentation of stimuli was intended to minimize the period of visual stimulation and the potential for eye movements. Blocks of mazes in each of the four directions were presented four times, yielding 16 blocks total. The maze path direction for a given block varied parametrically in a counterbalanced design (Cox 1958) such that each direction was preceded and followed by each other direction an equal number of times (Fig. 2). Subjects fixated a central point throughout the experiment, which lasted ~ 11 min. Prior to scanning, subjects practiced the task outside of the scanner. During scanning, subjects performed at $84 \pm 2.9\%$ correct (mean $\pm$ SEM, $N = 3$ subjects). All trials were analyzed.

Subjects were instructed not to make eye movements. Two subjects performed the task in the magnet while their eyes were monitored by an eye tracking system (Avotec Inc., Stuart, FL, USA). Eye movements were not observed, consistent with studies showing that humans (Chafee et al. 2002) and monkeys (Crowe et al. 2005) can perform the maze task using covert attention in the absence of eye movements.

Image acquisition

Imaging was performed on a 7 T magnet (Magnex Scientific, UK) equipped with a Varian Inova (Palo Alto, CA, USA) console and Siemens Symphony/Harmony (Erlangen, Germany) gradient amplifier. A 15-channel radio frequency coil with an opening for presentation of visual stimuli (Adriany et al. 2004) and home-built digital receiver for multi-channel acquisition were used.

T1-weighted anatomical images were acquired using inversion-recovery TurboFLASH. The acquisition bandwidth was 72 kHz, the matrix was 128×128, and the field-of-view (FOV) was 18.7 cm. The flip angle of the excitation pulse was 10°. For inversion, an adiabatic

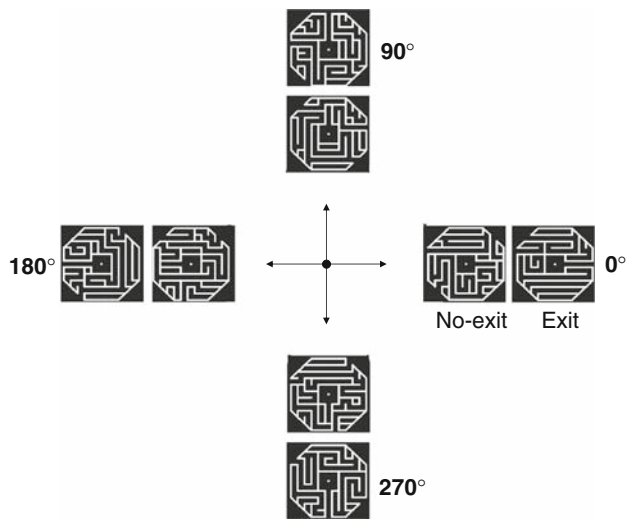

Fig. 1 Representative mazes shown; the directions of the maze path are shown in the *middle*

1	2	4	3
4	1	3	2
3	4	2	1
2	3	1	4

1 = 0°, 2 = 90°, 3 = 180°, 4 = 270°

Fig. 2 Counterbalanced experimental design. For the table illustrated, the order of presentation of maze path directions was *1*, *2*, *4*, *3*, *4*, *1*, *3*, *2*, *3*, *4*, *2*, *1*, *2*, *3*, *1*, *4*

hyperbolic secant pulse (HS4) (Tannus and Garwood 1996) with a bandwidth length product of 14 was applied. The inversion time was 1.45 s.

Seven oblique slices through the SPL were selected for each subject based on sagittal T1-weighted scout images. The slices were acquired without gaps. The fMRI time series were recorded using T2*-sensitized echo-planar imaging with an in-plane spatial resolution of 1.46 × 1.46 mm^2, a slice thickness of 2 mm, a TR of 1.5 s, and a TE of 25 ms. The flip angle was 60° and the acquisition bandwidth was 200 kHz.

A full FOV image (18.7 × 18.7 cm^2), from which the coil sensitivities were computed, was recorded before the functional time series. A matrix of 128 × 128 was obtained using four segments. The functional time series was acquired with reduced FOV consisting of one segment of the full FOV image (matrix: 128 × 32, FOV: 18.7 × 4.67 cm^2) corresponding to a one-dimensional reduction factor of 4. Images were reconstructed in Matlab using SENSE (Pruessmann et al. 1999; Moeller et al. 2006).

Data analysis

General

For each subject, the SPL was demarcated anteriorly by the postcentral sulcus, posteriorly by the lateral extension on the parietal-occipital sulcus, laterally by the medial edge of the intraparietal sulcus, and medially by the interhemispheric fissure. Data analyses were performed on single voxels within the SPL. The SPSS 15.0 statistical package for Windows (SPSS, Chicago, IL, USA; 2006), Matlab version 7.0 (Mathworks, Natick, MA, USA), and ad-hoc computer programs were used to implement the analyses.

Images were screened for motion artifacts by measuring variation in the center of mass of the functional images over the entire time course. This measurement was performed separately for the *X*, *Y*, and *Z* coordinates. Subject motion was further assessed by forming a cine loop of the images. Both measurements were performed using the fMRI analysis program STIMULATE (version 6.0.1, Center for Magnetic Resonance Research, University of Minnesota Medical School, Minneapolis, MN, USA) and motion correction was performed (Nestares and Heeger 2000).

A mask was applied to each voxel such that the coefficient of variation did not exceed 5% in order for that voxel to be analyzed further. This criterion was used because the coefficient of variation is higher in the vicinity of large vessels and outside of the brain (Kim et al. 1994). The data were log-transformed (Lewis et al. 2005; Yacoub et al. 2005) to meet the assumptions of parametric statistical analyses, namely normality, homoscedasticity, and additivity (Zar 1999). Finally, the data were detrended using a sliding regression algorithm to remove low frequency noise (Marchini and Ripley 2000).

For each voxel, an analysis of covariance (ANCOVA) was performed on the time series of SPL BOLD values. The first five time points for each block were discarded to allow the hemodynamic response to attain a steady state for that block. The dependent variable was the BOLD time series for each voxel, which consisted of 368 values (23 time points per block × 16 blocks). Fixed factors consisted of (1) the sequential Group of blocks, where each sequence of four blocks constituted a group (yielding four groups total), and (2) the maze path direction. If the maze path direction effect was statistically significant ($P < 0.05$), a sinusoidal multiple linear regression was performed to determine the presence of directional tuning (Georgopoulos et al. 1982):

$$A = b_0 + b_x \cos\,\theta + b_y \sin\,\theta + e$$

where A is BOLD activation, θ is maze path direction, b_0, b_x, and b_y are regression coefficients, and e is an error term. If either b_x or b_y were statistically significant, the 'preferred direction' (in radians) was calculated from the regression coefficients as arctan (b_y/b_x) and placed in the appropriate quadrant based on the sign of b_x and b_y. It was then converted to degrees and binned in eight bins using the four cardinal directions and the main diagonals as centers of the bins and a bin width of ±22.5°.

Permutation analysis

In the analyses above, many tests (ANOVAs and regressions) were carried out, since each was performed on data from each voxel. Therefore, it is possible that the percentage of directionally tuned voxels thus identified might be inflated. We evaluated this problem by performing a permutation analysis, as follows. For each voxel, the complete data set included 368 detrended time-course BOLD values (four maze path directions × 4 blocks × 23 images per block). These values were randomly permuted and all the statistical analyses were performed in the identical manner, as they were on the original, non-permuted data. This was done for each voxel. We wanted to determine the percentage of directionally tuned voxels following permutation.

Nearest neighbor analysis

In this analysis, we calculated the minimum distance between each voxel and the voxel with a reference preferred direction in the range $d \pm 22.5°$, where d is a specific directional bin. Color-coded maps of these minimum distances were plotted for qualitative evaluation.

K-*means clustering analysis*

The method of *k*-means clustering (Matlab, version 7.0), based on squared Euclidean distance, was used to find three-dimensional clusters of voxels tuned to the same binned direction. This method requires that the number of clusters be specified. Additionally, initial cluster centroids must be provided although these will be modified as the algorithm progresses. The optimal number of clusters was determined by comparing clustering solutions with 10–20 clusters. For each number of clusters between 10 and 20 the *k*-means method was repeated 50 times with initial cluster centroids selected randomly from the range of voxel coordinates with uniform probability. From each group of 50 clustering solutions the optimal solution was chosen to be that with the smallest sum of within-cluster, voxel-to-centroid distances. The clustering solution with the highest average silhouette value was selected as having the optimal cluster count.

Visualization of 3D directional clusters

For each voxel cluster, singular value decomposition (Matlab version 7.0) was used on the voxel coordinates to determine the three (orthogonal) directions of maximum variance. Ellipsoids were plotted centered at each cluster centroid. The principal axes of each ellipsoid are parallel to the directions of maximum variance and have lengths equal to twice the standard deviation of the voxel coordinates projected on the corresponding directions.

Results

Directional tuning

Of a total of 30,027 voxels contained within the SPL of 3 subjects, 20,384 (67.9%) showed a significant directional effect in an ANOVA, and, of those, 15,456/20,384 (75.8%) were directionally tuned. With respect to the whole voxel population, 15,456/30,027 = 51.5% voxels were directionally tuned. An example of a directionally tuned voxel is shown in Fig. 3. In the permutation analysis (see Materials and methods), not even a single voxel (out of 30,027 total) showed a statistically significant tuning.

A color-coded map of the minimum distances calculated in the nearest neighbor analysis (see Materials and methods) is shown in Fig. 4 (single slice) and Fig. 5 (all slices from one subject). It can be seen that (1) voxels with similar preferred directions tended to cluster, (2) preferred directions were represented repeatedly, and (3) voxels with approximately opposite preferred directions tended to occupy complementary spaces in the SPL. The *k*-means clustering analysis (see Materials and methods), identified

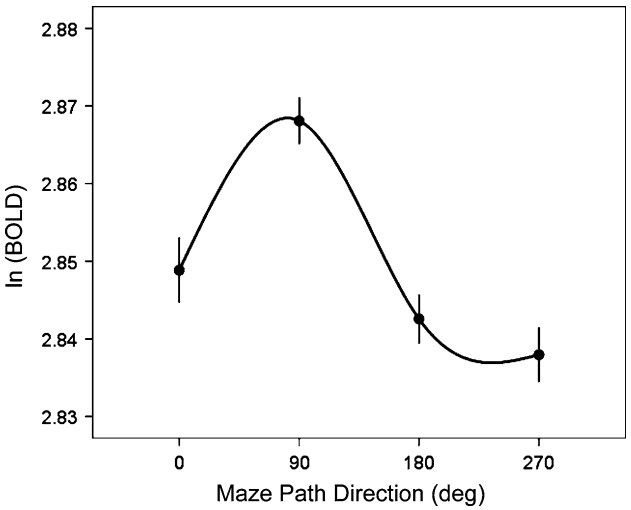

Fig. 3 Directional tuning curve of a single voxel in the left SPL. *Plotted points* are means (±SEM) of detrended BOLD signals. The sinusoidal function was: BOLD = 2.85 + 0.003 cos θ + 0.015 sin θ ($P < 10^{-7}$). The preferred direction was at 78.2°

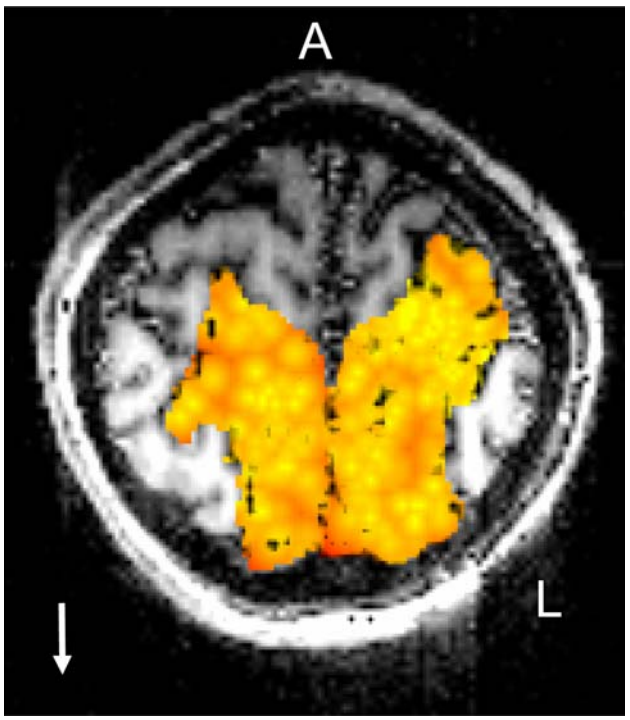

Fig. 4 Nearest neighbor plot for the downward (±22.5°) preferred direction (reference direction; *white arrow*) in a single slice of a subject (see Materials and methods). *Colored areas* indicate the SPL; the color variation, from *light yellow* → *red*, corresponds to short → long distances, respectively. Therefore, *light yellow areas* indicate high concentration of voxels tuned to the reference direction, whereas *dark red areas* denote absence of voxels tuned to the reference direction. *A* anterior; *L left*

3D clusters consisting of voxels with the same (binned) preferred direction. The spatial distribution of voxel clusters in three different directions in a hemisphere of one

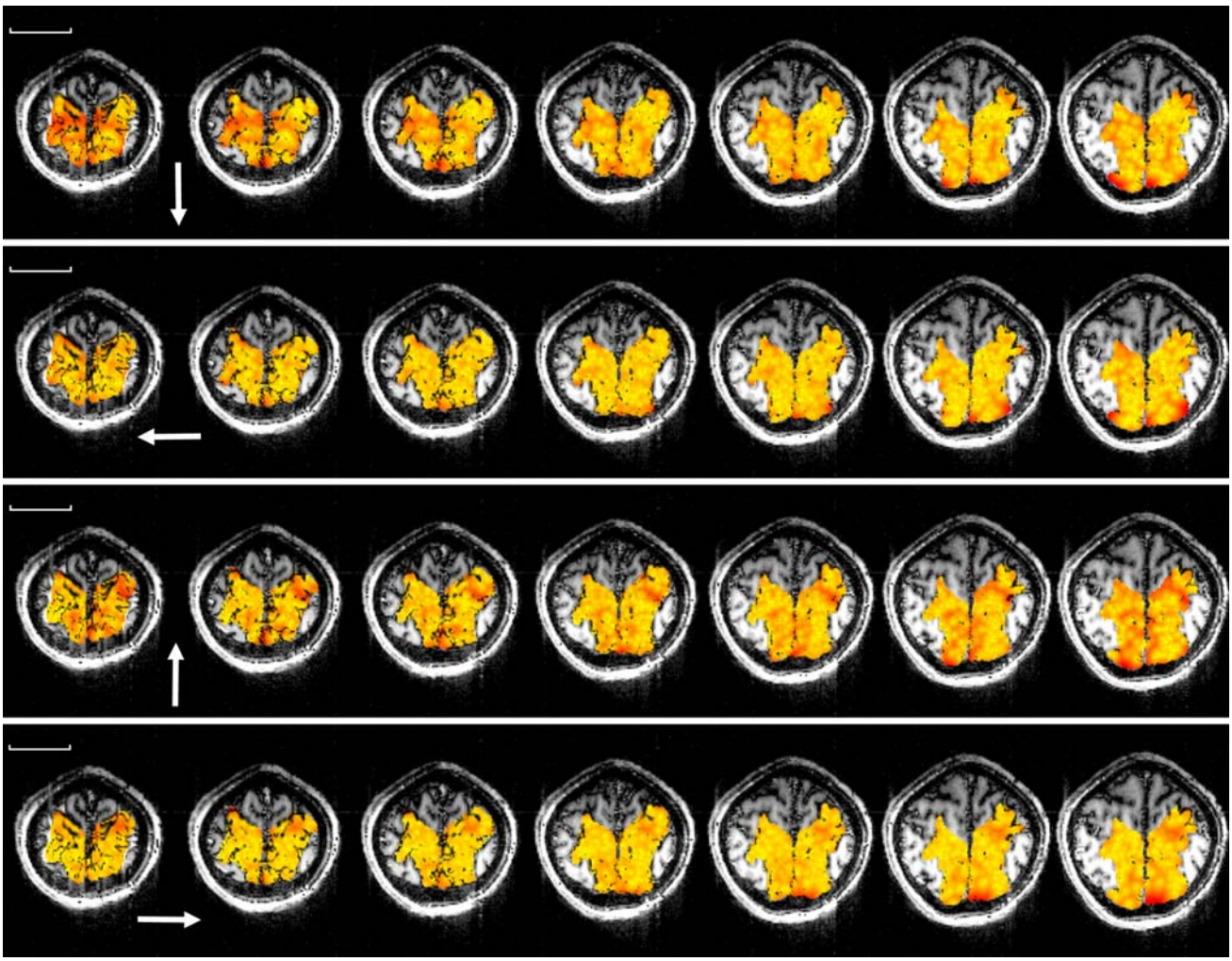

Fig. 5 Nearest neighbor plots for the four cardinal preferred directions in all slices of a single subject. *Scale bar* is 5 cm. Other conventions are as in Fig. 4

subject is shown in Fig. 6. The centers of all clusters in that same hemisphere are shown in Fig. 7. On the average (±SEM) there were 13.1 ± 0.48 same-direction clusters per hemisphere ($N = 3$ subjects × 2 hemispheres × 8 direction bins = 48) containing 22.5 ± 0.76 voxels per cluster ($N = 740$ clusters containing at least three voxels per cluster). The average minimum distance between the centers of same-direction (nearest neighbor) 3D clusters per hemisphere was 9.38 ± 0.25 mm ($N = 48$).

Discussion

Directional tuning was found in 51% of single voxels in the SPL with respect to the direction in which a maze was mentally traversed. Furthermore, directionally tuned voxels tended to cluster, such that voxels tuned to different directions were distributed throughout the SPL. These results are consistent with our previous study of mental maze solving using 4 T fMRI (Gourtzelidis et al. 2005). The present study extended those results by using a 7 T magnet, parallel imaging, greater spatial resolution (2 mm thick slices), and an experimental design tailored to the spatial-cognitive process under investigation. It is worth noting that, in the present context, "direction" refers to the shifting focus of attention with respect to the center of the maze and not to any physical movement. Moreover, the interdigitation of voxels of different preferred directions makes possible the local computation of the maze path direction. Indeed, previous analyses, using the neuronal population vector as an outcome of this process, have demonstrated that this is feasible (Gourtzelidis et al. 2005).

Methodological considerations: field strength, parallel imaging, and fMRI

Many studies have directly compared fMRI at low (1.5 T) and high (3–4 T) fields and documented an increase in

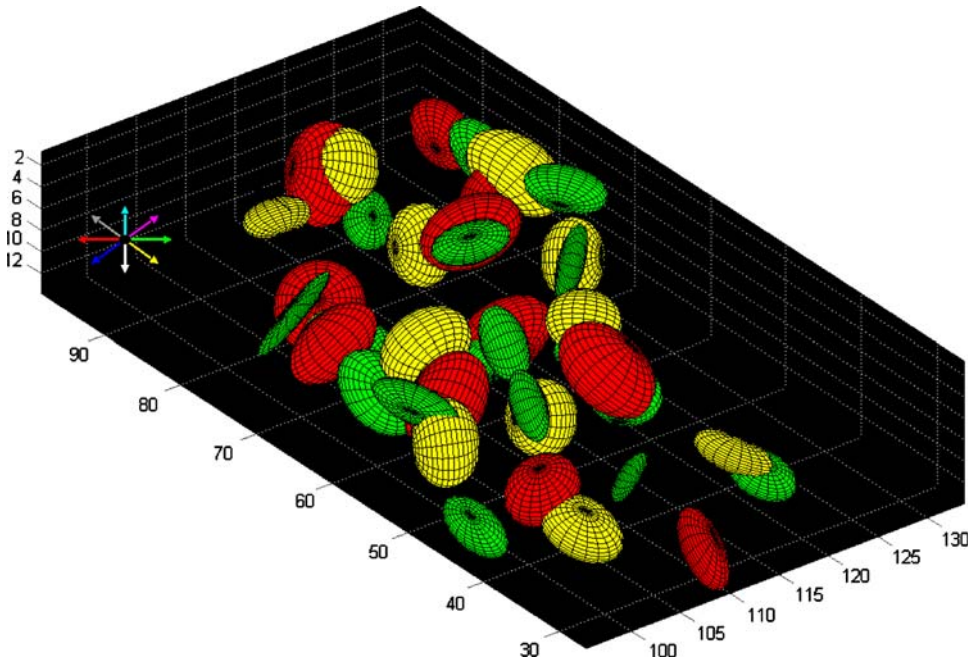

Fig. 6 Three dimensional plots of directional clusters for three color-coded preferred directions in the left hemisphere of a subject. See text for details. Axes are in mm

sensitivity at the higher field (for a review, see Voss et al. 2006). For example, Turner et al. (1993) presented visual stimuli and reported increases in image intensity in visual cortex of up to 7% at 1.5 T and 28% at 4 T. Gati et al. (1997) presented visual stimuli and found a linear relation between SNR and field strength, and a greater than linear relation between CNR and field strength for tissue but not for vessels in V1. In the motor system, Yang et al. (1999) found a 70% increase in the number of activated voxels and a 20% increase in *t* scores at 4 T compared to 1.5 T. Fera et al. (2004) examined a finger tapping task at 1.5 and 3 T and found a 59% increase in the number of activated voxels and an 18% increase in *t* scores at the higher field. Similarly, Yacoub et al. (2001) noted larger stimulation-induced changes in ΔR_2* and larger number of activated voxels at 7 T compared to 4 T for the same statistical significance (Yacoub et al. 2001). Employing motor and visual tasks, Krüger et al. (2001) found increases of 36 and 44% in the number of activated voxels in the motor and visual cortices, respectively, at 3 versus 1.5 T. Importantly, Krasnow

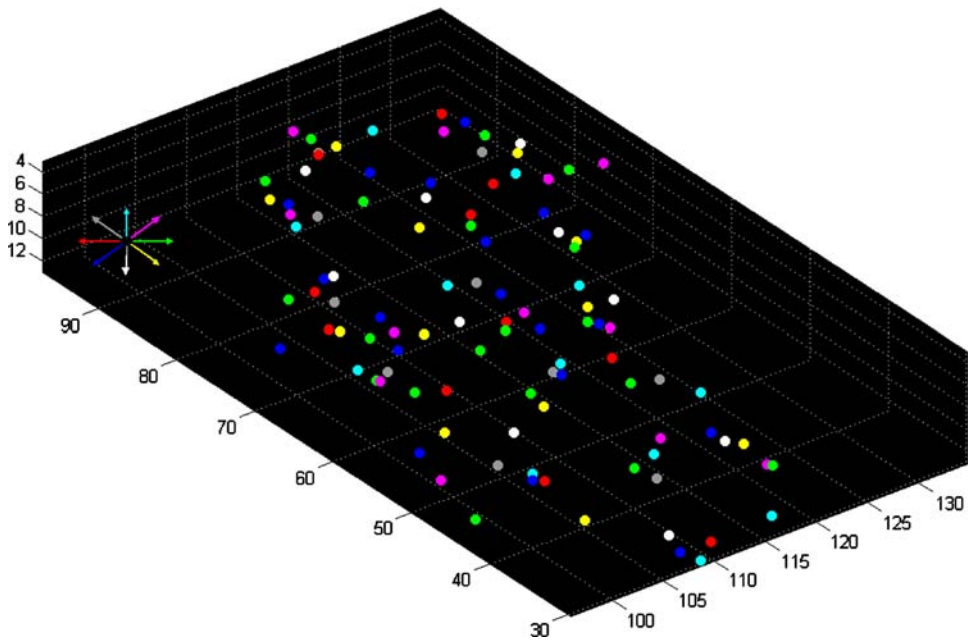

Fig. 7 Location of all cluster centers of all preferred directions in the same hemisphere as in Fig. 6

et al. (2003) and Hoenig et al. (2005) observed not only greater activation at 3 T than 1.5 T, but also activations in areas that were not detectable at 1.5 T. Likewise, Maldjian et al. (1999) demonstrated a somatotopic organization in sensorimotor cortex at 4 T that had not been consistently documented at 1.5 T, Formisano et al. (2003) identified a tonotopic map in human auditory cortex for the first time with fMRI at 7 T, and Yacoub et al. (2007) reported highly reproducible, robust detection of ocular dominance columns at 7 T (Yacoub et al. 2007).

Imaging at ultra-high fields such as 7 T provides a leap forward in both the sensitivity (SNR and CNR) and the spatial specificity of the BOLD signal with respect to the underlying neuronal response (Uğurbil 2002; Harel et al. 2006b). At 1.5 T, the BOLD signal mainly arises from blood-related effects associated with large vessels, whereas the contribution from capillaries is nearly undetectable (Lai et al. 1993; Frahm et al. 1994; Haacke et al. 1994; Boxerman et al. 1995; Song et al. 1996; Oja et al. 1999; Hoogenraad et al. 2001). Even at 3 T, the BOLD signal is dominated by blood and thus by large veins (Jochimsen et al. 2004). At 7 T and higher magnetic fields, the contribution by large vessels decreases and the signal from the microvasculature is readily detectable (Lee et al. 1999; Yacoub et al. 2001, 2003, 2005; Silva and Koretsky 2002; Duong et al. 2003; Harel et al. 2006a). The technical challenges of ultra-high field imaging can be offset by the benefits of parallel imaging (Ohliger et al. 2003; Wiesinger et al. 2004, 2006; Moeller et al. 2006). In parallel imaging, multiple receiver coils simultaneously acquire distinct spatial information, reducing the need for gradient encoding, which increases the speed of image acquisition and leads to the benefits enumerated in the Introduction. Together, ultra-high field fMRI and parallel imaging allow cognitive neuroscientists to investigate more refined attributes of sensory, cognitive, and motor processes, and to do so at a finer level of physiological detail. Additionally, some of the gain in sensitivity at ultra-high field can be spent to optimize other imaging parameters, such as reducing voxel size, which would minimize partial volume effects among other benefits. In the present study, we traded SNR for a voxel size and TR that are approximately half that of the typical fMRI experiment.

Functional layout of the PPC for attention

A wealth of evidence from neuropsychological (Critchley 1953), neurophysiological (Lynch et al. 1977), and functional neuroimaging (Pardo et al. 1991; Corbetta et al. 1993) studies has shown that the PPC is a key neural substrate of attention. In terms of the particular attentional operations subserved by regions within the PPC, neurophysiological studies in monkeys have produced important discoveries (Andersen et al. 1997; Colby and Goldberg 1999; Crowe et al. 2004; Chafee et al. 2007). Delineating the functional neuroanatomy of attention in the human PPC has been challenging, however, because considerable differences exist between the PPC of monkeys and humans (Hyvärinen 1982; Culham and Kanwisher 2001). Furthermore, the relatively course spatial and temporal resolution of neuroimaging methods, such as fMRI, has made fine-grained mapping difficult or unfeasible. Nevertheless, sophisticated experimental designs and analysis strategies, along with technical innovations in imaging hardware and software, have allowed investigators to begin to parse the functional neuroanatomy of attention. For example, Posner and Rothbart (2007) have identified three networks involved in alerting, orienting, and executive attention. The maze task used in the present study would seem to be most closely related to the orienting network, in which attention is allocated to locations in space. Functional imaging studies of attentional orienting have observed bilateral SPL activation (Corbetta et al. 1993; Hopfinger et al. 2000; Fan et al. 2005). Using tasks similar to attentional orienting, Yantis and colleagues have examined BOLD activation during shifts of attention to different locations (Yantis et al. 2002). It was found that the SPL and inferior parietal lobule (IPL) were transiently active when subjects shifted attention between spatial locations, whereas the SPL and intraparietal sulcus (IPS) showed consistently greater activation for shifts of attention to the contralateral periphery (Kelley et al. 2008). Such a contralateral bias in the PPC has often been reported in attention tasks, and a topographic map in the PPC for the contralateral visual hemifield has been reported (Sereno et al. 2001). This finding was extended by Silver et al. (2005), who provided evidence for two topographically organized areas in the IPS, each representing visuospatial attention in the contralateral visual field.

In the present study, we observed bilateral SPL activation during a task in which covert attention was mentally tracing radial paths emanating from the fixation point. The results of the present study, in conjunction with the results of our previous fMRI study of mental maze solving (Gourtzelidis et al. 2005), provide strong evidence that an elementary cognitive operation of attention, namely the direction of covert attention, is encoded by clusters of neurons distributed throughout the SPL. Furthermore, this effect is detectable by fMRI at the single-voxel level. The directional tuning of single voxels indicates that the associated BOLD intensity very probably reflects coherent, directionally selective synaptic activities of spatially close neuronal ensembles; on the other hand, the lack of tuning in a given voxel might suggest either a true absence of tuning or, alternatively, locations of transition in preferred directions, such that no coherent directionality is detected

by the BOLD signal. It should be emphasized that visual stimulation, motor responses, and the cognitive operation under investigation (covert attention) were identical on every trial in the current experiment; only the direction of attention changed. This design allowed us to attribute activation in single SPL voxels to the direction of attention, rather than relying on the comparison of a quiescent or non-task-related baseline to a task condition in order to infer directional tuning. Other studies may not have observed a directional effect for the following reasons. First, the effect is unquestionably more robust at high or ultra-high magnetic fields than at lower fields, especially when combined with other imaging techniques that maximize the MR signal. Second, the present study analyzed single voxels without spatial smoothing, brain normalization to a template, or analytical strategies such as the requirement that contiguous voxels be activated. Nearly all previous fMRI studies of covert attention have employed such procedures, which would be expected to blur the signal at the single-voxel level.

3D clustering of directional tuning in SPL

A major objective of this study was to accurately map the direction of mental tracing in the SPL. Previous work at 4 T (Gourtzelidis et al. 2005) had provided clear evidence for the orderly representation of this variable in the SPL. However, substantial uncertainty still remained concerning the true mapping parameters for the following reasons. First, the field at 4 T, although high, is still somewhat limited (with respect to SNR and CNR) for the intended high spatial resolution mapping. Second, the slice thickness of 5 mm in the previous study limited the potential mapping information in 3D brain space. And third, the use of control task in the tuning analysis increased the variability of the data, thus potentially blurring the tuning estimates. All of these concerns were addressed in the present study. Namely, the 7 T magnet provided adequate field strength for a substantially improved SNR and CNR. In addition, the higher field assured that the activation observed arose from local BOLD changes. This, in turn, allowed for mapping in high spatial resolution (2 mm slice thickness) which enabled an almost isotropic sampling of the brain ($1.46 \times 1.46 \times 2$ mm). Finally, the counterbalanced design implemented in this study dispensed of the need for a second (control) task and thus increased the sensitivity of the analysis.

The results obtained confirmed the earlier ones (Gourtzelidis et al. 2005) with respect to the presence of directional tuning of single voxels, the multiple representation of preferred directions, and the clustering of same-direction voxels. However, a major new result was the visualization of the directional tuning in 3D brain space (Figs. 6, 7). To our knowledge, this is the first time that this has been achieved. We attribute this achievement to the enhanced sensitivity and spatial accuracy of the MR signal provided by the higher magnetic field used in the present study and consequently the reduced partial volume effects that would tend to obfuscate the directional tuning. The observation that roughly half of the SPL voxels were directionally tuned is consistent with a neurophysiological study of monkeys performing a nearly identical task (Crowe et al. 2004), in which about half of the single cells recorded in PPC were tuned to the maze-path direction. The nearest-neighbor plots in the current study (Figs. 4, 5), which display concentrations of voxels tuned to a reference direction, were much more fine-grained than those obtained at 4 T (see Figs. 8, 9 in Gourtzelidis et al. 2005), and have a honeycomb organization. This result almost undoubtedly reflects the greater spatial specificity of the BOLD signal at 7 T with respect to the underlying neuronal activity. Consistent with this result, Raffi and Siegel (2005) reported a patchy topographical arrangement in the PPC using optical imaging that correlated with a monkey's locus of spatial attention. Our fMRI results in humans, in combination with the results of neurophysiological (Crowe et al. 2004) and optical imaging (Raffi and Siegel 2005) studies of monkeys in the inferior parietal lobule (an area thought to be homologous to the human SPL), provide converging evidence that spatially close neuronal ensembles in the PPC code for the direction of covert visuospatial attention. Of course, further research is needed to elucidate these questions. For example, regarding the direction of attention, it remains to be investigated whether directional tuning for attention is observed for directions outside of the visual field (e.g. behind the head), for other stimulus modalities (e.g. audition), and in other areas of the brain. fMRI at ultra-high fields such as 7 and now 9.4 T (Vaughn et al. 2006) holds great promise for contributing to this research.

Acknowledgments We thank Dr. Cheryl Olman for assistance with motion correction. This work was supported by NIH RR08079, BTRR P41 008079, Neuroscience P30 NS057091, the MIND Institute, the KECK Foundation, the United States Department of Veterans Affairs, and the American Legion Chair in Brain Sciences.

References

Adriany G, Van de Moortele P-F, Ritter J, Strupp JP, Snyder C, Moeller S, Andersen PM, Vaughan JT, Uğurbil K (2004) An elliptical open-faced transceive array for ultra high field parallel imaging and fMRI applications. In: Proceedings of 12th annual meeting ISMRM, Kyoto, Japan, p 1604

Andersen RA, Snyder LH, Bradley DC, Xing J (1997) Multimodal representation of space in the posterior parietal cortex and its use in planning movements. Annu Rev Neurosci 20:303–330

Boxerman JL, Bandettini PA, Kwong KK, Baker JR, Davis TL, Rosen BR, Weisskoff RM (1995) The intravascular contribution to fMRI signal change: Monte Carlo modeling and diffusion-weighted studies in vivo. Magn Reson Med 34:4–10

Brown RE, Clements RL (1999) 100 years of mazes in psychology and neuroscience. Soc Neurosci Abstr 25:261

Chafee MV, Averbeck BB, Crowe DA, Georgopoulos AP (2002) Impact of path parameters on maze solution time. Arch Ital Biol 140:247–251

Chafee MV, Averbeck BB, Crowe DA (2007) Representing spatial relationships in posterior parietal cortex: single neurons code object-referenced position. Cereb Cortex 17:2914–2932

Colby CL, Goldberg ME (1999) Space and attention in parietal cortex. Annu Rev Neurosci 22:319–349

Corbetta M, Miezin FM, Shulman GL, Petersen SE (1993) A PET study of visuospatial attention. J Neurosci 13:1202–1226

Cox DR (1958) Planning of experiments. Wiley, New York

Critchley M (1953) The parietal lobes. Edward Arnold, London

Crowe DA, Averbeck BB, Chafee MV, Anderson JH, Georgopoulos AP (2000) Mental maze solving. J Cogn Neurosci 12:813–827

Crowe DA, Chafee MV, Averbeck BB, Georgopoulos AP (2004) Neural activity in primate parietal area 7a related to spatial analysis of visual mazes. Cereb Cortex 14:23–34

Crowe DA, Averbeck BB, Chafee MV, Georgopoulos AP (2005) Dynamics of parietal neural activity during spatial cognitive processing. Neuron 47:885–891

Culham JC, Kanwisher NG (2001) Neuroimaging of cognitive functions in human parietal cortex. Curr Opin Neurobiol 11:157–163

Duong TQ, Yacoub E, Adriany G, Hu X, Uğurbil K, Kim SG (2003) Microvascular BOLD contribution at 4 and 7 T in the human brain: gradient-echo and spin-echo fMRI with suppression of blood effects. Magn Reson Med 49:1019–1027

Fan J, McCandliss BD, Fossella J, Flombaum JI, Posner MI (2005) The activation of attentional networks. Neuroimage 26:471–479

Fera F, Yongbi MN, van Gelderen P, Frank JA, Mattay VS, Duyn JH (2004) EPI-BOLD fMRI of human motor cortex at 1.5 T and 3.0 T: sensitivity dependence on echo time and acquisition bandwidth. J Magn Reson Imaging 19:19–26

Formisano E, Kim DS, Di Salle F, van de Moortele PF, Uğurbil K, Goebel R (2003) Mirror-symmetric tonotopic maps in human primary auditory cortex. Neuron 40:859–869

Frahm J, Merboldt KD, Hanicke W, Kleinschmidt A, Boecker H (1994) Brain or vein–oxygenation or flow? On signal physiology in functional MRI of human brain activation. NMR Biomed 7:45–53

Gati JS, Menon RS, Uğurbil K, Rutt BK (1997) Experimental determination of the BOLD field strength dependence in vessels and tissue. Magn Reson Med 38:296–302

Gati JS, Menon RS, Rutt BK (1999) Field strength dependence of functional MRI signals. In: Moonen CTW, Bandettini PA (eds) Functional MRI. Springer, Berlin, pp 277–282

Georgopoulos AP, Kalaska JF, Caminiti R, Massey JT (1982) On the relations between the direction of two-dimensional arm movements and cell discharge in primate motor cortex. J Neurosci 2:1527–1537

Gourtzelidis P, Tzagarakis C, Lewis SM, Crowe DA, Auerbach E, Jerde TA, Uğurbil K, Georgopoulos AP (2005) Mental maze solving: directional fMRI tuning and population coding in the superior parietal lobule. Exp Brain Res 165:273–282

Haacke EM, Hopkins A, Lai S, Buckley P, Friedman L, Meltzer H, Hedera P, Friedland R, Klein S, Thompson L, Detterman D, Tkach J, Lewin JS (1994) 2D and 3D high resolution gradient echo functional imaging of the brain: venous contributions to signal in motor cortex studies. NMR Biomed 7:54–62

Harel N, Lin J, Moeller S, Uğurbil K, Yacoub E (2006a) Combined imaging-histological study of cortical laminar specificity of fMRI signals. Neuroimage 29:879–887

Harel N, Uğurbil K, Uludag K, Yacoub E (2006b) Frontiers of brain mapping using MRI. J Magn Reson Imaging 23:945–957

Hoenig K, Kuhl CK, Scheef L (2005) Functional 3.0-T MR assessment of higher cognitive function: are there advantages over 1.5-T imaging? Radiology 234:860–868

Hoogenraad FG, Pouwels PJ, Hofman MB, Reichenbach JR, Sprenger M, Haacke EM (2001) Quantitative differentiation between BOLD models in fMRI. Magn Reson Med 45:233–246

Hopfinger JB, Buonocore MH, Mangun GR (2000) The neural mechanisms of top-down attentional control. Nat Neurosci 3:284–291

Hyvarinen J (1982) Posterior parietal lobe of the primate brain. Physiol Rev 62:1060–1129

Jochimsen TH, Norris DG, Mildner T, Moller HE (2004) Quantifying the intra- and extravascular contributions to spin-echo fMRI at 3 T. Magn Reson Med 52:724–732

Kelley TA, Serences JT, Giesbrecht B, Yantis S (2008) Cortical mechanisms for shifting and holding visuospatial attention. Cereb Cortex 18:114–125

Kim SG, Hendrich K, Hu X, Merkle H, Uğurbil K (1994) Potential pitfalls of functional MRI using conventional gradient-recalled echo techniques. NMR Biomed 7:69–74

Krasnow B, Tamm L, Greicius MD, Yang TT, Glover GH, Reiss AL, Menon V (2003) Comparison of fMRI activation at 3 and 1.5 T during perceptual, cognitive, and affective processing. Neuroimage 18:813–826

Krüger G, Kastrup A, Glover GH (2001) Neuroimaging at 1.5 T and 3.0 T: comparison of oxygenation-sensitive magnetic resonance imaging. Magn Reson Med 45:595–604

Lai S, Hopkins AL, Haacke EM, Li D, Wasserman BA, Buckley P, Friedman L, Meltzer H, Hedera P, Friedland R (1993) Identification of vascular structures as a major source of signal contrast in high resolution 2D and 3D functional activation imaging of the motor cortex at 1.5T: preliminary results. Magn Reson Med 30:387–392

Lee SP, Silva AC, Uğurbil K, Kim SG (1999) Diffusion-weighted spin-echo fMRI at 9.4 T: microvascular/tissue contribution to BOLD signal changes. Magn Reson Med 42:919–928

Lewis SM, Jerde TA, Tzagarakis C, Gourtzelidis P, Georgopoulos MA, Tsekos N, Amirikian B, Kim SG, Uğurbil K, Georgopoulos AP (2005) Logarithmic transformation for high-field BOLD fMRI data. Exp Brain Res 165:447–453

Lynch JC, Mountcastle VB, Talbot WH, Yin TC (1977) Parietal lobe mechanisms for directed visual attention. J Neurophysiol 40:362–389

Maldjian JA, Gottschalk A, Patel RS, Detre JA, Alsop DC (1999) The sensory somatotopic map of the human hand demonstrated at 4 Tesla. Neuroimage 10:55–62

Marchini JL, Ripley BD (2000) A new statistical approach to detecting significant activation in functional MRI. Neuroimage 12:366–380

Menon RS, Ogawa S, Tank DW, Uğurbil K (1993) 4 Tesla gradient recalled echo characteristics of photic stimulation-induced signal changes in the human primary visual cortex. Magn Reson Med 30:380–386

Moeller S, Van de Moortele PF, Goerke U, Adriany G, Uğurbil K (2006) Application of parallel imaging to fMRI at 7 Tesla utilizing a high 1D reduction factor. Magn Reson Med 56:118–129

Molenberghs P, Mesulam MM, Peeters R, Vandenberghe RR (2007) Remapping attentional priorities: Differential contribution of superior parietal lobule and intraparietal sulcus. Cereb Cortex 17:2703–2712

Nestares O, Heeger DJ (2000) Robust multiresolution alignment of MRI brain volumes. Magn Reson Med 43:705–715
Nitz DA (2006) Tracking route progression in the posterior parietal cortex. Neuron 49:747–756
Ohliger MA, Grant AK, Sodickson DK (2003) Ultimate intrinsic signal-to-noise ratio for parallel MRI: electromagnetic field considerations. Magn Reson Med 50:1018–1030
Oja JM, Gillen J, Kauppinen RA, Kraut M, van Zijl PC (1999) Venous blood effects in spin-echo fMRI of human brain. Magn Reson Med 42:617–626
Olton DS (1979) Mazes, maps, and memory. Am Psychol 34:583–596
Pardo JV, Fox PT, Raichle ME (1991) Localization of a human system for sustained attention by positron emission tomography. Nature 349:61–64
Porteus SD (1969) A psychologist of sorts: the autobiography and publications of the inventor of the Porteus maze tests. Pacific Books, Oxford
Posner MI, Rothbart MK (2007) Research on attention networks as a model for the integration of psychological science. Annu Rev Psychol 58:1–23
Pruessmann KP, Weiger M, Scheidegger MB, Boesiger P (1999) SENSE: sensitivity encoding for fast MRI. Magn Reson Med 42:952–962
Raffi M, Siegel RM (2005) Functional architecture of spatial attention in the parietal cortex of the behaving monkey. J Neurosci 25:5171–5186
Richter W, Somorjai R, Summers R, Jarmasz M, Menon RS, Gati JS, Georgopoulos AP, Tegeler C, Uğurbil K, Kim SG (2000) Motor area activity during mental rotation studied by time-resolved single-trial fMRI. J Cogn Neurosci 12:310–320
Scannell JW, Young MP (1999) Neuronal population activity and functional imaging. Proc Biol Sci 266:875–881
Segebarth C, Belle V, Delon C, Massarelli R, Decety J, Le Bas JF, Decorps M, Benabid AL (1994) Functional MRI of the human brain: predominance of signals from extracerebral veins. Neuroreport 5:813–816
Sereno MI, Pitzalis S, Martinez A (2001) Mapping of contralateral space in retinotopic coordinates by a parietal cortical area in humans. Science 294:1350–1354
Shmuel A, Yacoub E, Chaimow D, Logothetis NK, Uğurbil K (2007) Spatio-temporal point-spread function of fMRI signal in human gray matter at 7 Tesla. Neuroimage 35:539–552
Silva AC, Koretsky AP (2002) Laminar specificity of functional MRI onset times during somatosensory stimulation in rat. Proc Natl Acad Sci USA 99:15182–15187
Silver MA, Ress D, Heeger DJ (2005) Topographic maps of visual spatial attention in human parietal cortex. J Neurophysiol 94:1358–1371
Sodickson DK, Manning WJ (1997) Simultaneous acquisition of spatial harmonics (SMASH): fast imaging with radiofrequency coil arrays. Magn Reson Med 38:591–603
Song AW, Wong EC, Tan SG, Hyde JS (1996) Diffusion weighted fMRI at 1.5 T. Magn Reson Med 35:155–158
Tagaris GA, Kim S-G, Strupp JP, Andersen P, Uğurbil K, Georgopoulos AP (2000) Mental rotation studied by functional magnetic resonance imaging at high field (4 Tesla): performance and cortical activation. J Cogn Neurosci 9:419–432
Tannús A, Garwood M (1996) Improved performance of frequency-swept pulses using offset-independent adiabaticity. J Mag Res Ser A 120:133–137
Tolman EC (1932) Purposive behavior in animals and men. The Century Co., New York
Turner R, Jezzard P, Wen H, Kwong KK, Le Bihan D, Zeffiro T, Balaban RS (1993) Functional mapping of the human visual cortex at 4 and 1.5 Tesla using deoxygenation contrast EPI. Magn Reson Med 29:277–279
Uğurbil K (2002) High-field magnetic resonance. In: Toga AW, Mazziotta JC (eds) Brain mapping: the methods, 2nd edn. Academic Press, London, pp 291–313
Uğurbil K, Toth L, Kim DS (2003) How accurate is magnetic resonance imaging of brain function? Trends Neurosci 26:108–114
Uğurbil K, Chen W, Harel N, Van de Moortele P-F, Yacoub E, Zhu XH, Uludag K (2006) Magnetic resonance imaging of brain function. In: Akay M (eds) Wiley encyclopedia of biomedical engineering. Wiley, Hoboken, pp 647–668
Vandenberghe R, Gitelman DR, Parrish TB, Mesulam MM (2001) Functional specificity of superior parietal mediation of spatial shifting. Neuroimage 14:661–673
Vaughan T, DelaBarre L, Snyder C, Tian J, Akgun C, Shrivastava D, Liu W, Olson C, Adriany G, Strupp J, Andersen P, Gopinath A, van de Moortele PF, Garwood M, Uğurbil K (2006) 9.4T human MRI: preliminary results. Magn Reson Med 56:1274–1282
Voss HU, Zevin JD, McCandliss BD (2006) Functional MR imaging at 3.0 T versus 1.5 T: a practical review. Neuroimaging Clin N Am 16:285–297
Wiesinger F, Van de Moortele PF, Adriany G, De Zanche N, Uğurbil K, Pruessmann KP (2004) Parallel imaging performance as a function of field strength—an experimental investigation using electrodynamic scaling. Magn Reson Med 52:953–964
Wiesinger F, Van de Moortele PF, Adriany G, De Zanche N, Uğurbil K, Pruessmann KP (2006) Potential and feasibility of parallel MRI at high field. NMR Biomed 19:368–378
Yacoub E, Shmuel A, Pfeuffer J, Van De Moortele P-F, Adriany G, Andersen P, Vaughan JT, Merkle H, Uğurbil K, Hu X (2001) Imaging brain function in humans at 7 Tesla. Magn Reson Med 45:588–594
Yacoub E, Duong TQ, Van De Moortele PF, Lindquist M, Adriany G, Kim SG, Uğurbil K, Hu X (2003) Spin-echo fMRI in humans using high spatial resolutions and high magnetic fields. Magn Reson Med 49:655–664
Yacoub E, Van De Moortele PF, Shmuel A, Uğurbil K (2005) Signal and noise characteristics of Hahn SE and GE BOLD fMRI at 7 T in humans. Neuroimage 24:738–750
Yacoub E, Shmuel A, Logothetis N, Uğurbil K (2007) Robust detection of ocular dominance columns in humans using Hahn Spin Echo BOLD functional MRI at 7 Tesla. Neuroimage 37:1161–1177
Yang Y, Wen H, Mattay VS, Balaban RS, Frank JA, Duyn JH (1999) Comparison of 3D BOLD functional MRI with spiral acquisition at 1.5 and 4.0 T. Neuroimage 9:446–451
Yantis S, Schwarzbach J, Serences JT, Carlson RL, Steinmetz MA, Pekar JJ, Courtney SM (2002) Transient neural activity in human parietal cortex during spatial attention shifts. Nat Neurosci 5:995–1002
Zar JH (1999) Biostatistical analysis (fourth edition). Prentice Hall, Inc., Upper Saddle River
Zou KH, Greve DN, Wang M, Pieper SD, Warfield SK, White NS, Manandhar S, Brown GG, Vangel MG, Kikinis R, Wells WM III (2005) Reproducibility of functional MR imaging: preliminary results of prospective multi-institutional study performed by biomedical informatics research network. Radiology 237:781–789